Appl Phys A (2009) 96: 33–42
DOI 10.1007/s00339-009-5178-2

Applied Physics A
Materials Science & Processing

Molecular dynamics simulations of laser-induced damage of nanostructures and solids

Harald O. Jeschke · Momar S. Diakhate · Martin E. Garcia

Received: 20 November 2008 / Accepted: 27 February 2009 / Published online: 17 March 2009

Abstract A theoretical approach to treat laser induced femtosecond structural changes in covalently bonded nanostructures and solids is described. Our approach consists in molecular dynamic simulations performed on the basis of time-dependent, many-body potential energy surfaces derived from tight-binding Hamiltonians. The shape and spectral composition of the laser pulse is explicitly taking into account in a non-perturbative way. We show a few examples of the application of this approach to describe the laser damage and healing of defects in carbon nanotubes with different chiralities and the ultrafast nonequilibrium melting of bulk germanium, initiated by the laser-induced softening and destabilization of transversal acoustic phonon modes.

PACS 71.15.Pd · 61.46.-w · 64.70.D · 78.47.-p · 78.47.J-

1 Introduction

The interaction of femtosecond laser pulses and solids gives rise to a large variety of novel and interesting effects, including nonthermal structural changes. Laser pulses of durations ranging from a few femtoseconds up to half a picosecond and intensities above 10^{12} W/cm^2 may induce lattice instabilities which lead to thermal and nonthermal structural transformations.

H.O. Jeschke
Institut für Theoretische Physik, Goethe-Universität Frankfurt, Max-von-Laue-Str. 1, 60438 Frankfurt, Germany

M.S. Diakhate · M.E. Garcia (✉)
Theoretische Physik, Universität Kassel, Heinrich-Plett-Str. 40, 34132 Kassel, Germany
e-mail: magarcia@physik.uni-kassel.de
Fax: +49-561-8044006

In the last two decades, different types of laser induced reversible and irreversible ultrafast structural changes were observed, like excitation of coherent phonons [1–9] or nonequilibrium phase transitions, the latter including order–disorder [10, 11], solid–solid [12, 13] and solid–liquid [14–26] transformations.

Many different pump-probe techniques were used in the experiments mentioned above. In some works a laser pulse was used as a probe, and the time dependence of the reflectivity or the dielectric function was measured [27]. The development of sources of ultrashort X-ray pulses made it possible to perform time-resolved diffraction experiments [28] recording rocking curves as a function of time. This method has the advantage that it permits a direct visualization of the lattice dynamics upon laser excitation. Finally, in the last years time-resolved electron diffraction experiments were performed.

Most of the results obtained in the mentioned experiments show clear evidences of nonthermal structural changes as a consequence of intense femtosecond laser excitation.

Regarding the systems studied experimentally, a group of materials that merits particular attention includes semiconductors because of their technological significance. Of special interest are materials like silicon (Si), germanium (Ge) and gallium arsenide (GaAs) which are widely used in semiconductor devices; here short time behavior becomes even more important as the frequencies at which these devices are operated increase [18, 29]. The study of electronic relaxation time scales is very important for the development of nanodevices. Carbon nanotubes are potentially good candidates for future technological applications like ultrafast optical storage media or cluster assembled materials [30, 31]. Finally, covalent solids like diamond, graphite and other carbon materials like diamond-like carbon (DLC) are of enormous technological interest because of their physical prop-

erties including extreme hardness and very high thermal conductivity. For these materials there is a large field of research concerning ultrashort laser-induced modification, annealing, ablation and machining [32].

Covalent systems are also interesting from the viewpoint of basic research, since their structural response differs dramatically from that of metals. Femtosecond laser excitation of covalent solids exhibits new and interesting features. First, absorption of photons in covalent solids leads rapidly to bond-breaking processes. As soon as bonds are broken, the picture of electron-phonon coupling is no longer valid. Moreover, the concept of phonons becomes meaningless, since the potential landscape cannot be represented any more by a superposition of harmonic potentials. As a consequence, the widely used two-temperature model breaks down and a different theoretical approach is necessary. Such an approach must take into account explicitly the atomic coordinates and must yield a correct description of the bonding. In this paper we will describe in detail a microscopic theory for laser-induced structural changes in covalent solids.

Despite the intensive experimental activities, only a few theoretical methods were developed in the last years to describe laser induced structural changes.

The pioneer works by Stampfli and Bennemann [33–35] were very successful in describing the laser-induced lattice destabilization in Si, Ge and C and constituted the basis for the theoretical approach presented here. Stampfli and Bennemann analyzed the instabilities caused by the electron–hole plasma in terms of one or two phonon degrees of freedom, and assuming that the entropy of the excited electrons remains constant during and after laser heating. By assuming the instant creation of an electron–hole plasma of a given density ξ at a time $t = 0$, the duration of the laser pulse is set to zero ($\tau = 0$). Other approaches make use of molecular dynamics (MD) simulations based on model potentials, like the Stillinger–Weber potential for the case of Si [36]. However, and as we show below, model interatomic potentials which do not include the electrons as degrees of freedom are not optimally suited for a theoretical treatment of laser-induced structural changes. Recently, this drawback of model potentials was compensated by introducing the electron dynamics in the framework of the two-temperature molecular dynamics model [37]. This improved approach works well for metals, but not for covalent systems.

Parrinello and coworkers employed first principles MD simulations [38–40]. These are based upon a treatment of the electrons and ions in the lattice with density functional theory in the local density approximation and with plane waves as basis functions. The volume of the MD cell was kept constant. The numerical cost of such calculations is very high [40], so that these methods would not permit a study of many different laser intensities and durations on various materials as was the intention of this work. Concerning the results obtained for the laser melting of graphite [41], it seems possible that the choice of a constant volume MD method imposed too severe a restriction on the relaxation channels available to the material. These authors also assume for their melting studies the instant creation of a high electron temperature T_e at a time $t = 0$. Thus, the laser pulses are taken to be delta functions of duration $\tau = 0$ which makes it impossible to analyze the influence of the pulse duration. A similar approach as the one described above, but using a tight-binding basis instead of Kohn–Sham functions has been used by Ho and coworkers [42].

The method which will be presented in the next section was developed by us to study laser excitation of diamond, graphite and silicon in the bulk [43–47] and in ultrathin films [48, 49], C_{60} clusters [50], and carbon nanotubes [51, 52].

Independently of our studies Allen and coworkers developed a similar method to describe the excitation of coherent phonons and laser-induced melting [53, 54]. This method is suitable for the study of the first few femtoseconds after excitation, since the assumption of constant volume is made and it is assumed that the electronic system does not undergo decoherence and thermalization processes after laser excitation.

The aim of our investigations is to understand on which time scale do laser-induced structural transitions occur, which relaxation channels are present and whether these relaxation channels be controlled by laser parameters like intensity, duration, and light frequency.

An important question which we attempt to answer is if there are fundamental differences between laser-induced and thermally induced bond breaking and phase transitions.

Important aspects taken into account in our theory are

(a) The admission of all relaxation channels in the response to an electron–hole plasma, including the calculation for all degrees of freedom and the admission of changes in sample volume and geometry
(b) The handling of the electronic nonequilibrium caused by strong laser excitation and its subsequent equilibration and relaxation, and
(c) The treatment of laser pulses with finite durations $\tau > 0$

In this paper we present a sketch of the theory and its application to the dynamics of single-walled carbon nanotubes (CNT) with defects upon femtosecond laser excitation and the ultrafast nonthermal melting of Ge.

2 Theory

Our model for the femtosecond laser excitation of covalent solids is based on the following physical picture: the

light pulses used in most of experiments interact primarily with the electronic system. A laser pulse of moderate intensity produces the excitation of electrons from occupied to unoccupied levels. This creation of electron–hole pairs occurs with a time-dependent probability which is proportional to the (time-dependent) intensity of the laser field. As a consequence of the extremely fast excitation process, a nonequilibrium distribution of electrons is created. Through electron–electron collisions the nonequilibrium electronic state thermalizes and an equilibrium (Fermi-like) distribution of the occupation of the electronic levels is reached rapidly. In our approach the electronic distribution thermalizes to a single chemical potential. The assumption of two separate chemical potentials for electrons and holes is only valid at very low fluences and for very small displacements of the ions. Our study deals with high laser intensities, which generate a very large amount of electron–hole pairs. Therefore, the phase space for recombination increases dramatically, and the recombination times become very short. In addition, when ions undergo large displacements, the electronic band structure is affected and crossings between the valence and the conduction bands become possible. These arguments were recently confirmed in a combined experimental and theoretical study of coherent phonons in bismuth, in which the assumption of a single chemical potential yields a better fit to experiments [9]. Parallel to the electron thermalization process, hot electron transport from the excited region into the rest of the material sets in. During this complex electron dynamics the lattice does not remain frozen, but might undergo bond breaking and restructuring processes. These structural changes may lead to another crystal phase, to melting or to ablation. We show in this section that the reason why the lattice structure undergoes changes upon laser heating is related to the rapid change in time of the potential energy surface $U(\{r_{ij}\},t)$ of the system when a large fraction of the electrons is excited. Note, that $U(\{r_{ij}\},t)$ is usually a very complex function of the interatomic distances $r_{ij}=|\mathbf{r}_i-\mathbf{r}_j|$ and, for most materials, cannot be written as a sum of pair potentials.

We describe laser-induced structural changes with the help of MD simulations. This means, that we treat the nuclear degrees of freedom of the problem classically. However, the electron dynamics must be treated quantum mechanically. The forces acting on the atoms are obtained as $\mathbf{F}_i(t)=-\nabla_i U(\{r_{ij}\},t)$ and cause the lattice dynamics, described by Newton's equations of motion.

2.1 "Laser-induced" potential energy surface

MD simulations constitute a standard method to study structural properties of solids in thermodynamical equilibrium. In this situation, the potential energy surface $U(\{r_{ij}\})$ is usually approximated by model potentials, like, for example, Lennard–Jones [55], Tersoff [56] or Stillinger–Weber [57], which consist of functions of the interatomic distances r_{ij}.

For the description of laser-induced structural changes, however, such model potentials are not useful, since they do not contain the electrons as degrees of freedom. Therefore, they do not allow any reasonable description of the excitation process. As mentioned at the beginning of this section, the laser pulse interacts first with the electrons. Hence, for the studies to be presented in this paper, the many-body potential energy surface $U(\{r_{ij}\},t)$ must be derived from a microscopic electronic Hamiltonian.

We assume that the valence electrons of the covalent solid can be described by an effective single-particle Hamiltonian $H_{\rm eff}$ in a restricted Hilbert space spanned by M functions. $H_{\rm eff}$ depends, of course, on the electronic degrees of freedom, but also on the interatomic distances r_{ij}, since the properties of the electrons change if the r_{ij} change. The effect of the rest of the core electrons and the internuclear repulsion is approximated by a repulsive potential $E_{\rm rep}(\{r_{ij}\})$. As effective Hamiltonian for carbon and germanium we use

$$H=\sum_{i\alpha}\epsilon_{i\alpha}n_{i\alpha}+\sum_{ij\alpha\beta j\neq i}V_{ij}^{\alpha\beta}(r_{ij})c_{i\alpha}^{+}c_{j\beta}. \tag{1}$$

Here, $\epsilon_{i\alpha}$ is the on-site energy of atom i and orbital α. $c_{i\alpha}^{+}$ and $c_{j\alpha}$ are the creation and annihilation operators, and $V_{ij}^{\alpha\beta}(r_{ij})$ the hopping integrals. For the description of C and Ge, the ls, lp_x, lp_y and lp_z orbitals are taken into account ($l=2$ for C, $l=4$ for Ge). For the radial part $R(r)$ of the hopping integrals and for $E_{\rm rep}$ for C we employ the forms and parameterizations proposed by Xu et al. [58], in which, as usual in Tight-Binding (TB) methods the basis functions are assumed to be orthogonal to each other. For the case of Ge, however, a TB Hamiltonian based on orthogonal functions does not yield a proper description of the electronic and mechanical properties of the solid in equilibrium. Therefore, we follow in this case the idea developed by Harrison and Schilfgaarde [59], in which the effect of nonorthogonality is introduced via a proportional relationship between the overlap matrix element and Hamiltonian matrix elements. For the particular case of Ge a set of parameters yielding very good agreement with the experimental quantities has been already determined [60]. We use in this paper an improved version of this set of TB matrix elements.[1]

The most important fact of the TB Hamiltonian is that the matrix elements (and the overlaps in the case of nonorthogonal basis functions) depend on the interatomic distances r_{ij}.

The effective single-particle Hamiltonian $H_{\rm eff}(\{r_{ij}\})$ (1) yields M eigenvalues ϵ_m, which clearly depend on $\{r_{ij}\}$. The

[1] Details of the determination of the TB parameters and of the calculations of forces and phonon frequencies will be published elsewhere.

procedure to determine the eigenvalues is different for orthogonal and nonorthogonal basis functions.

If we assume that electron thermalization is very fast compared with the time scale for the motion of the ions, then the time-dependent potential energy surface $U(\{r_{ij}\},t)$ which governs the motion of the atoms will be equal to the free energy of the electrons $F_{\mathrm{el}}(\{r_{ij}\},t)$, and given by

$$U\big(\{r_{ij}\},t\big) = F_{\mathrm{el}}\big(\{r_{ij}\},t\big) = \sum_m n(\epsilon_m,t)\epsilon_m + E_{\mathrm{rep}}\big(\{r_{ij}\}\big) - T_{\mathrm{el}}(t)S_{\mathrm{el}}(t), \tag{2}$$

where $n(\epsilon_m,t)$ are the occupations of the corresponding electronic levels ϵ_m. This assumption of fast electron thermalization is justified for laser pulse intensities that excite a significant percentage of the valence electrons to the conduction band; such pulses that can induce rapid bond breaking and structural changes are the focus of our study. Due to the presence of the laser pulse, these occupations are time dependent, as we show below. The first term of (2) represents the attractive contribution from the valence electrons. The third term contains the electronic temperature T_{el} and the electronic entropy S_{el}, which is given by

$$S_{\mathrm{el}} = -k_B \sum_m \big[n(\epsilon_m,t)\log\big(n(\epsilon_m,t)\big) + \big(1-n(\epsilon_m,t)\big)\log\big(1-n(\epsilon_m,t)\big)\big]. \tag{3}$$

Equation (2) represents a generalization of the Born–Oppenheimer approximation (BOA). Note that the usual BOA is recovered for $T_{\mathrm{el}} = 0$.

It is important to point out that the functional dependence of $U(\{r_{ij}\},t)$ on the interatomic distances $\{r_{ij}\}$ is strongly dominated by the electronic occupations $n(\epsilon_m,t)$ present in the first and third terms of (2). If the electronic occupations undergo strong changes, then the potential energy landscape $U(\{r_{ij}\},t)$ will change significantly.

In view of the above discussion one can understand the mechanisms for laser-induced structural changes by using a simple physical picture sketched in Fig. 1. Before laser heating the solid is in thermodynamical equilibrium at a low initial (lattice and electronic) temperature ($T_i \leq 300$ K). This means that electrons fill mainly the states below the Fermi level. The resulting ground state potential landscape $U(\{r_{ij}\})$ shows minima at the crystal lattice sites. Atoms are sitting on these sites and therefore no forces act on them. However, the situation changes dramatically when the solid becomes heated by a laser pulse. For moderate and high fluences the laser creates a considerable amount of electron–hole pairs, as illustrated in Fig. 1. This means that the electronic occupations $n(\epsilon_m,t)$ change. Consequently, the functional form of $U(\{r_{ij}\})$ undergoes quantitative and qualitative changes, which results in the disappearance or shifting

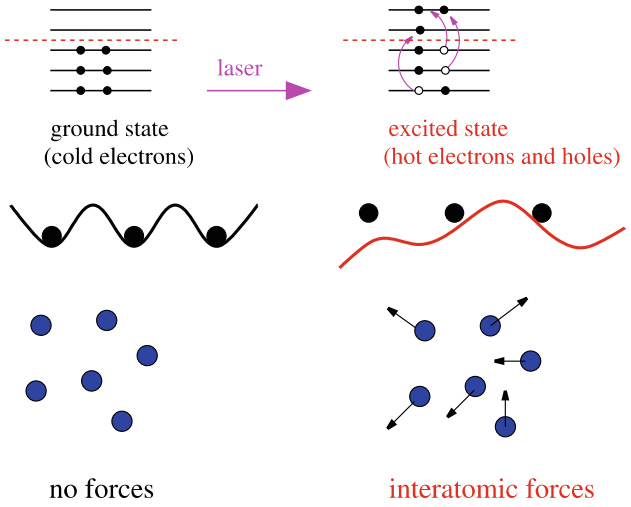

Fig. 1 Illustration of the microscopic physical picture derived from (2). (**a**) Situation before the action of the laser pulse: the solid is in thermodynamical equilibrium. For low temperatures, the electrons fill the states up to the Fermi level. The atoms are at the equilibrium positions of the ground state potential energy surface. (**b**) The laser pulse changes the electronic occupations. This leads to rapid changes in the potential energy landscape. As a consequence, the lattice becomes unstable and forces appear on the atoms, driving a structural change

of the minima. Since these modifications occur on a time scale which is much shorter than the reaction time of the lattice, the atoms remain in their positions, most of them no longer minima of the new potential landscape. Therefore, forces now act on the atoms, which start to move. This is the way laser-induced structural changes take place.

Figure 1 does not show how the electron occupations changes in time. This is a fundamental point, which must be taken carefully into account by any theory aimed at the description of laser-induced structural effects. In order to obtain an equation for the rate of change of the electron occupations $n(\epsilon_m,t)$ we consider the equation of motion for the density matrix $\hat{\rho}$, which reads

$$\dot{\hat{\rho}} = -\frac{i}{\hbar}\big[H_{\mathrm{TB}} + V_{\mathrm{laser}}, \hat{\rho}\big] + \left.\frac{\partial\hat{\rho}}{\partial t}\right|_{\mathrm{coll}}. \tag{4}$$

The first term refers to the coherent motion of the electrons, which is driven by the laser field and which involves optical transitions between the energy levels of the Hamiltonian H_{TB}. Since the tight-binding Hamiltonian is a single-particle one, it does not describe interactions between the excited electrons, which are essential for the thermalization processes. Thus, we treat them by including a second, dissipative term in (4).

Equation (4) represents a system of coupled differential equations for the diagonal and nondiagonal elements of the density matrix. However, since the electron–hole plasma created by the laser undergoes rapid dephasing, the relevant equations of motion will be those describing the diagonal

elements. Therefore, neglecting the contribution of the non-diagonal elements one obtains

$$\frac{dn(\epsilon_m,t)}{dt} = \int_{-\infty}^{\infty} d\omega\, g(\omega,t-\tau)\big\{\big[n(\epsilon_m-\hbar\omega,t-\tau) + n(\epsilon_m+\hbar\omega,t-\tau) - 2n(\epsilon_m,t-\tau)\big]\big\} - \frac{n(\epsilon_m,t)-n^0(\epsilon_m,T_{\mathrm{el}})}{\tau_1}. \quad (5)$$

Here, the first (integral) term describes the laser excitation and creation of a nonequilibrium electron distribution. $g(\omega,t)$ is the intensity function of the laser pulse, which describes the intensity as a function of frequency and time as a product of the time envelope and its Fourier transform. Thus, the electronic distribution is at each time step folded with the current intensity function $g(\omega,t)$. This means that, at each time step, the occupation of an energy level ϵ_m changes in proportion to the occupation difference with respect to levels at $\epsilon_m - \hbar\omega$ and at $\epsilon_m + \hbar\omega$. In (5) the optical matrix elements are assumed to be equal to unity, so that the band structure plays the main role in the absorption process. This simplification makes sense, as the calculation of optical matrix elements is at the same time tedious and known to be rather inaccurate in the TB approximation. Equation (5) can be straightforwardly generalized to include the dipole matrix elements. The second term of (5) describes the electron thermalization resulting from electron–electron collisions through a relaxation time τ_1. Thus, with a time constant τ_1, the distribution $n(\epsilon_m,t)$ approaches a Fermi–Dirac distribution $n^0(\epsilon_m,T_{\mathrm{el}})$, which is given by

$$n^0(\epsilon_m,T_{\mathrm{el}}) = \frac{1}{\exp\{\beta(\epsilon_m-\mu)+1\}}, \quad \text{with } \beta = \frac{1}{k_{\mathrm{B}}T_{\mathrm{el}}}. \quad (6)$$

Here, T_{el} is the electron temperature, and μ is the chemical potential. This simple approach works very well because for dense electron–hole plasmas in covalent solids extremely low relaxation times τ_1 have been found. A carrier thermalization faster than 10 fs in GaAs has been reported [61]. Even studies that use significantly lower laser intensities than are studied here find thermalization times of the order of 100 fs [62, 63]. Thus, we use $\tau_1 = 10$ fs for germanium. For carbon nanotubes, we expect the carrier thermalization to be somewhat slower, and we use $\tau_1 = 50$ fs. Note, for these short thermalization times the exact electronic dynamics leading to electronic equilibrium do not play a significant role for the structural changes we are studying here.

The electronic temperature T_{el} and the chemical potential μ, which appear in the Fermi–Dirac distribution and which are not determined by (5), need to be fixed by an additional principle. We will demand that the nonequilibrium distribution $n(\epsilon_m,t)$ approaches the Fermi-Dirac distribution while conserving the total energy of the system. Energy loss mechanisms, which are of course already present as soon as some laser energy has been absorbed, will be treated in a way that does not interfere with this principle of energy-conserving equilibration. The total energy at time t is required to be

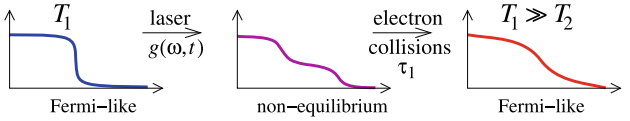

Fig. 2 Illustration of the electron excitation and thermalization processes described by (5). The electronic temperature T_2 reached after thermalization is much higher than the initial temperature T_1, since the electron system has absorbed energy from the laser pulse

$$E_{\mathrm{tot}}(t) = U\big(\{r_{ij}(t)\},t\big) + E_{\mathrm{kin}}(t) \stackrel{!}{=} E_{\mathrm{tot}}(t=0) + E_{\mathrm{abs}}(t) - E_{\mathrm{loss}}(t), \quad (7)$$

where $E_{\mathrm{kin}}(t)$ is the kinetic energy of the ions, and $E_{\mathrm{abs}}(t)$ is the energy that has been absorbed from the laser pulse up to the time t. A further, obvious demand which is necessary to determine T_{el} and μ is that the number of electrons N_{e} stays constant over the entire calculation:

$$N_{\mathrm{e}}(t) = \sum_m n(\epsilon_m,t) \stackrel{!}{=} N_{\mathrm{e}}^0. \quad (8)$$

Thus, by enforcing conservation of energy during the electron thermalization we make sure that we get physically meaningful results. In Fig. 2 the processes of excitation and thermalization are illustrated.

With this approach the effect of a laser-induced electronic nonequilibrium on the structural response can be studied. This theory for the time dependence of the occupation numbers would be too simple if electron dynamics during the first few femtoseconds after laser excitation were in the centre of our study. However, the main focus of this work are laser-induced structural changes on a time scale of a few picoseconds. These are not expected to be very sensible to fine details of the nonequilibrium distribution created by the laser pulse. Thus, (5) is used for the study of the dependence of structural relaxation on duration, frequency and intensity of the exciting pulses.

2.1.1 Summary of the numerical approach

Our theoretical description of laser-induced structural changes requires to solve in a parallel way the classical equations of motion for the nuclear degrees of freedom (and also of the lattice vectors, in the case of simulations at constant pressure [64, 65]) and the equations of motion for the

electronic occupations (5). The equations of motion are, of course, coupled. Changes in the occupations lead to changes in the potential energy surface. These lead to changes in the atomic coordinates (due to the presence of forces on the atoms) which cause changes in the eigenvalue spectrum of the Hamiltonian H_{TB} (due to changes of the hopping matrix elements). It is important to mention, that for each time step of our simulations we have to diagonalize H_{TB} and also solve (7) and (8) to determine the instantaneous electron temperature and chemical potential. The calculations of the forces acting on the ions as a gradient of the potential energy surface is rather straightforward in the case of orthogonal basis functions, but becomes technically more complicated for nonorthogonal functions.[2]

3 Results

In this section we show, as an example, results obtained using the model and the method described in the previous section. In this work we specifically discuss MD simulations we performed to investigate the femtosecond laser excitation of carbon nanotubes with topological defects and of bulk germanium.

3.1 Laser-induced damage and defect repair in carbon nanotubes

Carbon nanotubes are self-assembled nanostructures and usually exhibit defects which are formed during growth. Among the different types of defects which are present in CNT, particularly interesting ones are the so called topological, or Stone–Wales defects [66–69]. They consist of modifications of the geometric arrangements of lattice structure, conserving the total number of carbon atoms as in a perfect CNT. For instance, a pentagon–heptagon defect consists in the transformation of four hexagons belonging to the CNT into two pentagons and two heptagons. Such a defect can be easily rationalized in terms of a 90 deg rotation of a carbon dimer [70]. The defected CNT is in a local minimum of the potential energy surface and is separated from the global minimum (perfect hexagonal structure of the CNT) by a large energy barrier [71]. For all technical purposes, the defected CNT is a stable state and cannot be repaired by thermal annealing, because the corresponding temperature would be so high that, instead of producing healing, many new defects would be created.

According to the physics of laser-induced structural changes outlined in the previous section, the following question arises immediately: is it possible to achieve a laser-induced healing of topological defects in CNTs?

[2]Details of the determination of the TB parameters and of the calculations of forces and phonon frequencies will be published elsewhere.

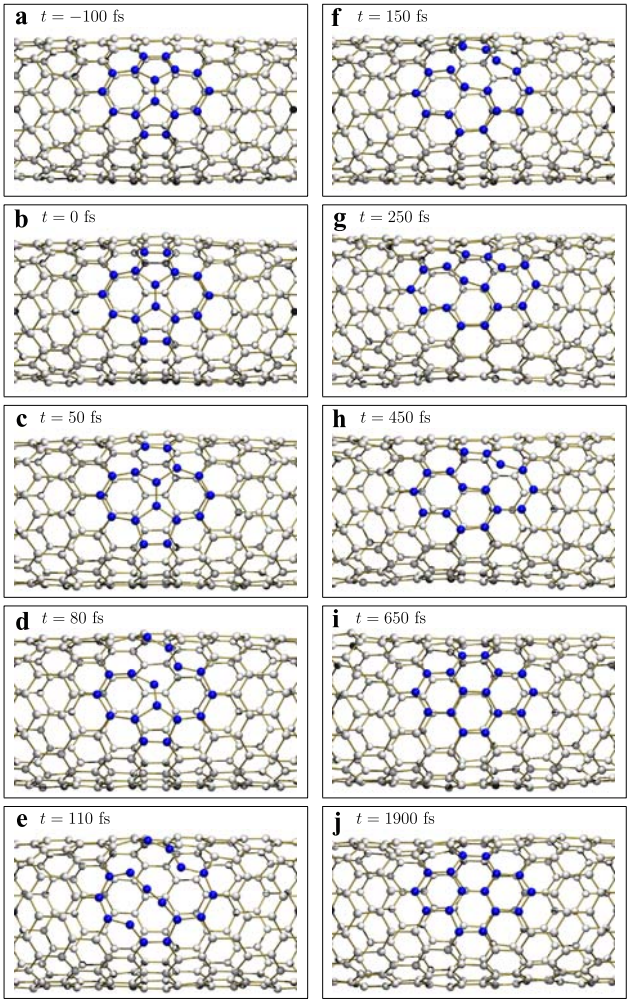

Fig. 3 Snapshots of the healing of a defective SWNT. For better visibility, the defect region with a single pentagon–heptagon defect is highlighted by darker atom colors (all atoms are carbon). An energy of $E_0 = 1.8$ eV/atom was absorbed from the pulse of $\tau = 50$ fs duration. The time zero coincides with the pulse maximum

To answer this question we performed systematic MD simulations for different laser pulse intensities using the method described in Sect. 2.

In the following we show that, in contrast to what occurs during thermal heating, the elimination of defects upon femtosecond laser excitation is possible due to the extreme nonequilibrium state created by the ultrashort intense laser pulses. We also determine which conditions must be fulfilled by the laser pulse so that healing is effective.

Figures 3(a)–(j) shows the healing of a (12,0) zigzag nanotube with a single pentagon–heptagon defect. The defect area is highlighted by darker coloring. The simulation was performed with variable periodic boundary conditions, allowing the single-wall nanotube (SWNT) to expand also in longitudinal direction upon laser excitation. At $t = 0$ fs, the time of the laser pulse maximum (see Fig. 3(b)), the absorption of part of the laser light already leads to bond

softening and thus expansion of the tube length and diameter. At $t = 50$ fs (see Fig. 3(c)), this has led to some bond breaking in the defect region. The absorbed energy of $E_0 = 1.8$ eV/atom is close to but below the damage threshold of the pristine (12,0) SWNT at this pulse duration. This means that the absorbed energy can break only the weaker bonds of the pentagon–heptagon defect. Further bond breaking (see Figs. 3(d) and (e)) free the carbon dimer which in the defect is rotated by 90° compared to the defect free SWNT gains the freedom to rearrange. Note, that this movement has a significant out-of-plane component. Due to strong vibrational excitation and suppression of the energy barrier that prevents the dimer rotation in equilibrium, Figs. 3(f)–(h) show back and forth rotation of the dimer before the pristine atomic arrangement stabilizes at $t = 650$ fs (see Fig. 3(i)) with all broken bonds repaired.

In Figs. 4(a)–(j), we demonstrate the effect of a somewhat higher laser intensity compared to Fig. 3, acting on the same (12,0) zigzag SWNT with a pentagon–heptagon defect. The absorption of an energy of $E_0 = 2.0$ eV/atom from the pulse leads to irreversible bond breaking in the defect region, causing four carbon atoms to be ejected. The dynamics starts out similar as in Fig. 3 with breaking of bonds of the pentagons and heptagons of the defect. The central dimer of the defect shows a very fast rotation towards its orientation in the pristine tube, but the laser excitation causes one atom to leave the SWNT already between $t = 100$ fs and $t = 150$ fs (it is not any more shown in Fig. 4(c)). Three more carbon atoms are ejected from the SWNT in the ensuing violent vibrational dynamics (see Fig. 4(d)–(g)). Finally, the central carbon dimer of the pentagon–heptagon defect stabilizes in its stable position, forming two hexagons (see Fig. 4(j)). This trajectory demonstrates that defects in SWNTs represent predetermined breaking points, allowing a selective action of a suitably chosen laser pulse.

Figure 5 shows the behavior of a chiral (9,2) SWNT slightly above the damage threshold. The number of atoms was $N = 412$. This threshold was determined to be $E_0 = 1.9 \pm 0.1$ eV/atom [72]. The chiral SWNTs with a diameter of $d \approx 8$ Å had shown roughly similar damage thresholds, but the (9,2) SWNT was slightly more susceptible to laser-induced damage at the $\tau = 20$ fs pulse duration used for this calculation. The trajectory of Fig. 5(a)–(f) was calculated with an energy of $E_0 = 2.1$ eV/atom absorbed from the pulse. The strong breathing mode activated by the pulse with maximum at $t = 0$ fs leads to first bond breaking at $t = 110$ fs (see Fig. 5(b)). Subsequently, two atoms are ejected from a tear in the SWNT wall on the left side of the shown tube section, and one atom from a tear on the right. In Fig. 5(f), the resulting holes are highlighted by darker shading of the atoms bordering the hole.

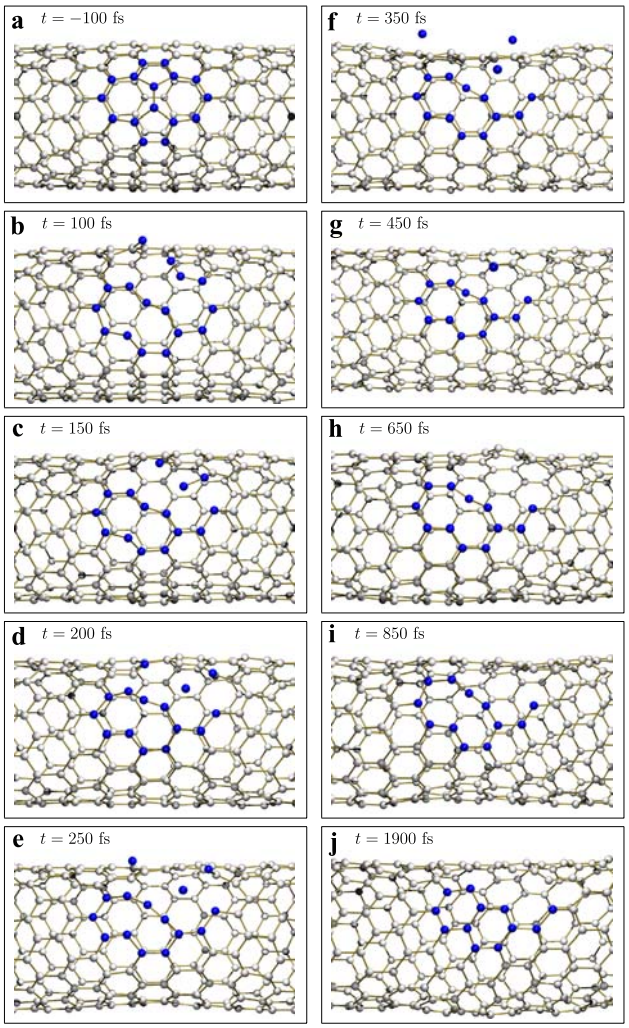

Fig. 4 Snapshots of laser-induced damage in a defective SWNT. For better visibility, the defect region with a single pentagon–heptagon defect is highlighted by darker atom colors (all atoms are carbon). An energy of $E_0 = 2.0$ eV/atom was absorbed from the pulse of $\tau = 50$ fs duration. The time zero coincides with the pulse maximum

3.2 Ultrafast melting of Ge

The second example we have chosen in order to show how our MD simulations can describe laser-induced nonequilibrium structural changes is the nonthermal melting of Ge. As mentioned in the previous section, Ge cannot be described by a set of orthogonal basis functions in the framework of a tight-binding model. Therefore, we extended the description to nonorthogonal functions and also performed two types of calculations in order to analyze the problem from different perspectives. First we determined the phonon spectrum of bulk Ge. For that, we used the frozen phonon method as implemented in the FROPHO code [73] in the framework of

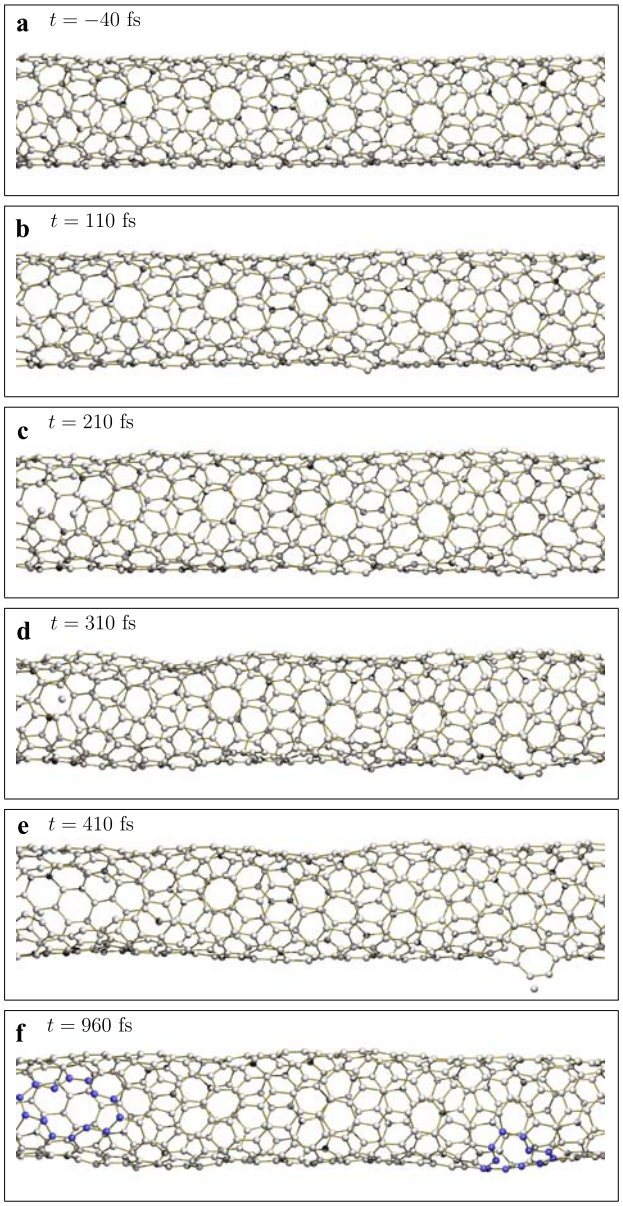

Fig. 5 Snapshots of laser-induced damage in a chiral (9,2) SWNT. An energy of $E_0 = 2.1$ eV/atom was absorbed from a laser pulse with FWHM of $\tau = 20$ fs. Laser-induced bond breaking causes the emission of three C atoms from two independent tears in the SWNT wall. In panel (**f**), the atoms surrounding the newly created vacancies are highlighted for clarity by darker atom colors (all atoms are carbon)

the nonorthogonal TB Hamiltonian used.[3] We calculated the phonon frequencies of Ge in the electronic ground state, i.e., at $T_{\mathrm{el}} = 0$ and compared them to the experimentally determined phonon spectrum [74]. Figure 6 shows, for the example of one transverse acoustic (TA) branch, that we obtain a good agreement with experiment. This makes us confident

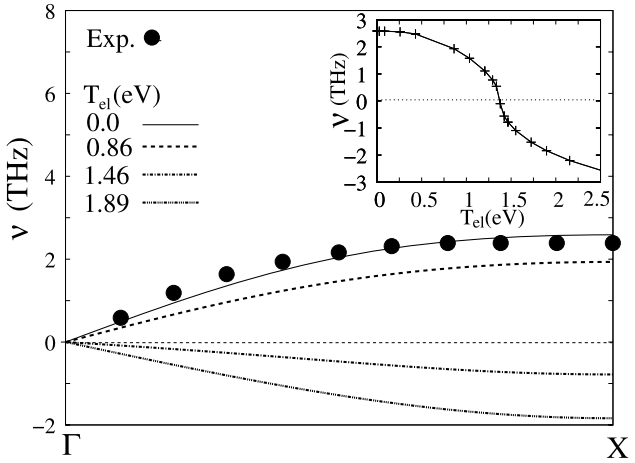

Fig. 6 Transverse acoustic (TA) phonons from Γ to X in the first Brillouin zone at different values of electronic temperature (T_{el}). Pure imaginary frequencies are plotted as negative. The *points* in the main figure are experimental values taken from [74]. The *inset* represents the frequency variation at the X point as function of T_{el}

that the nonorthogonal TB method yields a correct description. Now, we performed the same type of calculation, but assuming the electrons to be at a high temperature T_{el} in order to simulate the laser excitation. The results are presented in Fig. 6 as well. One can clearly observe how the TA phonons undergo a dramatic softening as the electronic temperature (i.e., the laser intensity) increases. Moreover, for high enough values of T_{el} the TA frequencies become purely imaginary in the range between the Γ and the X points of the Brillouin zone. This means that the potential surface along this direction and for all the k points in between becomes repulsive. A particular case is shown in the inset of the figure, in which the softening and the transition to a pure imaginary frequency is shown for the TA mode at the X point. This is in agreement with the predictions of Stampfli and Bennemann for silicon [35].

Although the laser-induced softening of particular phonon branches gives us important information about the first stages of the melting of Ge, it is necessary to perform MD simulations in order to learn more about the time scale of the melting process. Therefore we performed MD simulations using a supercell consisting of 64 atoms.

In order to follow the dynamics of melting of Ge we calculated, as a function of time after excitation, the bond angle distribution function. The bond angle is defined as the angle between two interatomic vectors joining a given atom in the cell. For the determination of the bond angle a cut-off distance of 3.2 Å was chosen, which is slightly beyond the position of the first peak of the pair correlation function.

The time-dependent bond angle distribution was calculated for different laser parameters (pulse duration, fluence, intensity). As an example, we show in Fig. 7 the calculated bond angle distribution as a function of time after

[3] Details of the determination of the TB parameters and of the calculations of forces and phonon frequencies will be published elsewhere.

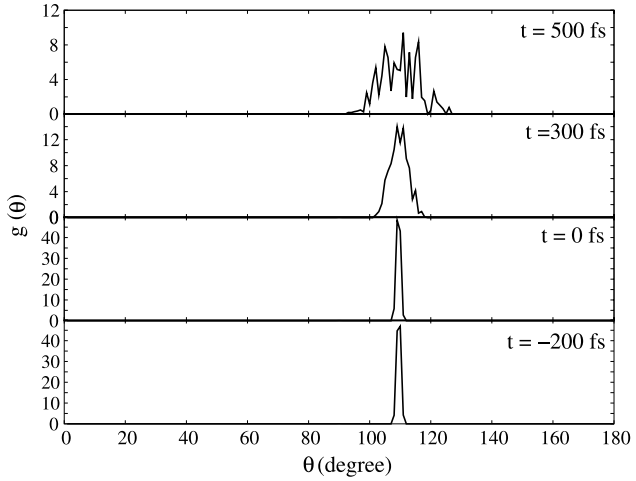

Fig. 7 Computed time evolution of the bond angle (see text) distribution after excitation with a laser pulse of $\tau = 130$ fs duration. The intensity of the pulse was chosen to reach an absorbed energy of 1.4 eV/atom

laser excitation. The pulse duration was $\tau = 130$ fs and the absorbed energy $E_0 = 1.4$ eV. The initial temperature of the crystalline Ge supercell was $T = 10$ K. Before the action of the laser pulse, the bond angle distribution shows a very sharp peak at 109 degrees, which gives evidence of the tetrahedral nature of the bond distribution in the initial diamond crystal structure of the cold Ge. As a consequence of laser excitation, however, the peak starts to broaden very rapidly. For a time delay of 500 fs the whole range of bond angles from 100 to 120 degrees can be found with high probability, which means that the crystalline ordering starts to be destroyed. According to our simulations the time scale for nonthermal melting is about half a picosecond.

4 Conclusions

We have presented a model and theory for the description of structural changes induced by a strong laser-induced nonequilibrium. Molecular dynamics calculations were performed on the basis of an electronic TB Hamiltonian. Applicability for electronic nonequilibrium is achieved with a method for the calculation of time-dependent occupation numbers of the eigenstates of the system. This leads to a method of performing MD calculations on time-dependent potential energy surfaces. The electronic nonequilibrium occupation is determined by the energy absorbed by the electrons during the action of the laser pulse. Therefore the nonequilibrium is a function of the pulse shape, frequency, intensity and duration. The return of the electronic system to equilibrium via electron–electron collisions is explicitly taken into account. The electron–lattice equilibration is treated with a Boltzmann-like approach. In this way, energy loss of the electronic system to the lattice via electron–phonon coupling and to the surrounding cold lattice via hot electron diffusion is taken into consideration. Thus, the theory can deal with the structural response of solids and clusters to the absorption of laser energy up to 10 or 100 ps.

The method was applied to SWNTs with pentagon–heptagon defects. The laser pulse with an intensity below the damage threshold of the pristine SWNT induces bond breaking especially in the defect region. We demonstrated that the free energy surface of the SWNT at the high electron temperatures produced by the absorption of energy from the laser pulse has a significantly lowered barrier for the repair of the pentagon–heptagon defect. Therefore, an intensity window for the laser aided repair of the defect exists.

As a second example, we analyzed the laser-induced nonthermal melting of Ge both from the point of view of the softening of phonon modes (static description) and also performing MD simulations applying the method outlined in this work. We could show how the nonthermal process starts by a dramatic reduction of the frequencies of the TA phonons. From the MD simulations we were able to determine the time scale on which nonthermal melting of Ge occurs.

Acknowledgements This work has been supported financially by the Deutsche Forschungsgemeinschaft (DFG) through the priority program SPP 1134 and by the BMBF through the Verbundprojekt FSP301-FLASH (FKZ: 05KS7SJ1). H.O. Jeschke acknowledges support by the DFT through the Emmy Noether program.

References

1. M. Hase, K. Ishioka, M. Kitajima, K. Ushida, S. Ishita, Appl. Phys. Lett. **76**, 1258 (2000)
2. K. Ishioka, M. Hase, M. Kitajima, K. Ushida, Appl. Phys. Lett. **78**, 3965 (2001)
3. M. Hase, M. Kitajima, S.-I. Nakashima, K. Mizoguchi, Phys. Rev. Lett. **88**, 067401 (2002)
4. C. Rose-Petruck, R. Jimenez, T. Guo, A. Cavalleri, C.W. Siders, F. Raksi, J.A. Squier, B.C. Walker, K.R. Wilson, C.P.J. Barty, Nature (Lond.) **398**, 310 (1999)
5. M. Hase, M. Kitajima, A.M. Constantinescu, H. Petek, Nature (Lond.) **426**, 51 (2003)
6. K. Sokolowski-Tinten, C. Blome, J. Blums, A. Cavalleri, C. Dietrich, A. Tarasevitch, I. Uschmann, E. Förster, M. Horn-von-Hoegen, D. von der Linde, Nature (Lond.) **422**, 287 (2003)
7. C. von Korff Schmising, M. Bargheer, M. Kiel, N. Zhavoronkov, M. Woerner, T. Elsaesser, I. Vrejoiu, D. Hesse, M. Alexe, Phys. Rev. Lett. **98**, 257601 (2007)
8. P. Gaal, W. Kuehn, K. Reimann, M. Woerner, T. Elsaesser, R. Hey, Nature (Lond.) **450**, 1210 (2007)
9. S.L. Johnson, P. Beaud, C.J. Milne, F.S. Krasniqi, E.S. Zijlstra, M.E. Garcia, M. Kaiser, D. Grolimund, R. Abela, G. Ingold, Phys. Rev. Lett. **100**, 155501 (2008)
10. K. Sokolowski-Tinten, J. Solis, J. Bialkowski, J. Siegel, C.N. Afonso, D. von der Linde, Phys. Rev. Lett. **81**, 3679 (1998)

11. J.P. Callan, A.M.-T. Kim, C.A.D. Roeser, E. Mazur, J. Solis, J. Siegel, C.N. Afonso, J.C.G. De Sande, Phys. Rev. Lett. **86**, 3650 (2001)
12. A. Cavalleri, C. Tóth, C.W. Siders, J.A. Squier, F. Ráksi, P. Forget, J.C. Kieffer, Phys. Rev. Lett. **87**, 237401 (2001)
13. F. Carbone, P. Baum, P. Rudolf, A.H. Zewail, Phys. Rev. Lett. **100**, 035501 (2008)
14. C.V. Shank, R. Yen, C. Hirlimann, Phys. Rev. Lett. **51**, 900 (1983)
15. H.W.K. Tom, G.D. Aumiller, C.H. Brito-Cruz, Phys. Rev. Lett. **60**, 1438 (1988)
16. D.H. Reize, H. Ahn, M.C. Downer, Phys. Rev. B **45**, 2677 (1992)
17. K. Sokolowski-Tinten, J. Bialkowski, D. von der Linde, Phys. Rev. B **51**, 14186 (1995)
18. A. Leitenstorfer, S. Hunsche, J. Shah, M.C. Nuss, W.H. Knox, Physica B **272**, 348 (1999)
19. R. Schoenlein, C. Chattopadhyay, H.H.W. Chong, T.E. Glover, P.A. Heimann, C.V. Shank, A. Zholents, M. Zolotorev, Science **287**, 2237 (2000)
20. C.W. Siders, A. Cavalleri, K. Sokolowski-Tinten, C. Tóth, T. Guo, M. Kammler, M. Horn von Hoegen, K.R. Wilson, D. von der Linde, C.P.J. Barty, Science **286**, 1340 (1999)
21. A.M. Lindenberg, I. Kang, S.L. Johnson, T. Missalla, P.A. Heimann, Z. Chang, X. Larsson, P.H. Bucksbaum, H.C. Kapteyn, H.A. Padmore, R.W. Lee, J.S. Wark, R.W. Falcone, Phys. Rev. Lett. **84**, 111 (2000)
22. A. Rousse, C. Rischel, S. Fournaux, I. Uschmann, S. Sebban, G. Grillon, P. Balcou, E. Förster, J.P. Gelndre, P. Audebert, J.C. Gauthier, D. Hulin, Nature (Lond.) **410**, 65 (2001)
23. A. Rousse, C. Rischel, J.C. Gauthier, Rev. Mod. Phys. **73**, 17 (2001)
24. S.L. Johnson, P.A. Heimann, A.M. Lindenberg, H.O. Jeschke, M.E. Garcia, Z. Chang, R.W. Lee, J.J. Rehr, R.W. Falcone, Phys. Rev. Lett. **91**, 157403 (2003)
25. A.M. Lindenberg, J. Larsson, K. Sokolowski-Tinten, K.J. Gaffney, C. Blome, O. Synnergren, J. Sheppard, C. Caleman, A.G. MacPhee, D. Weinstein, D.P. Lowney, T.K. Allison, T. Matthews, R.W. Falcone, A.L. Cavalieri, D.M. Fritz, S.H. Lee, P.H. Bucksbaum, D.A. Reis, J. Rudati, P.H. Fuoss, C.C. Kao, D.P. Siddons, R. Pahl, J. Als-Nielsen, S. Duesterer, R. Ischebeck, H. Schlarb, H. Schulte-Schrepping, Th. Tschentscher, J. Schneider, D. von der Linde, O. Hignette, F. Sette, H.N. Chapman, R.W. Lee, T.N. Hansen, S. Techert, J.S. Wark, M. Bergh, G. Huldt, D. van der Spoel, N. Timneanu, J. Hajdu, R.A. Akre, E. Bong, P. Krejcik, J. Arthur, S. Brennan, K. Luening, J.B. Hastings, Science **308**, 392 (2005)
26. M. Harb, R. Ernstorfer, Ch.T. Hebeisen, G. Sciaini, W. Peng, T. Dartigalongue, M.A. Eriksson, M.G. Lagally, S.G. Kruglik, R.J.D. Miller, Phys. Rev. Lett. **100**, 155504 (2008)
27. S.K. Sundaram, E. Mazur, Nat. Phys. **1**, 217 (2002)
28. D.A. Reis, M.F. DeCamp, P.H. Bucksbaum, R. Clarke, E. Dufresne, M. Hertlein, R. Merlin, R. Falcone, H. Kapteyn, M.M. Murnane, J. Larsson, Th. Missalla, J.S. Wark, Phys. Rev. Lett. **86**, 3072 (2001)
29. M.S. Sherwin, Curr. Opin. Solid State Mater. Sci. **3**, 191 (1998)
30. A. Perez, P. Melinon, V. Dupuis, P. Jensen, A. Prevel, J. Tuaillon, L. Bardotti, C. Martet, M. Treilleux, M. Broyer, M. Pellarin, J.L. Vaille, B. Palpant, J. Lerme, J. Phys. D **30**, 709 (1997)
31. M. Terrones, W.K. Hsu, H.W. Kroto, D.R.M. Walton, in *Fullerenes and Related Structures*, ed. by A. Hirsch. Topics in Current Chemistry, vol. 199 (Springer, Berlin, 1999)
32. F.P. Bundy, W.A. Bassett, R.S. Weathers, R.J. Hemley, H.K. Mao, A.F. Goncharov, Carbon **34**, 141 (1996)
33. P. Stampfli, K.H. Bennemann, Phys. Rev. B **42**, 7163 (1990)
34. P. Stampfli, K.H. Bennemann, Phys. Rev. B **46**, 10686 (1992)
35. P. Stampfli, K.H. Bennemann, Phys. Rev. B **49**, 7299 (1994)
36. R.F.W. Herrmann, J. Gerlach, E.E.B. Campbell, Appl. Phys. A **66**, 35 (1998)
37. D.S. Ivanov, L.V. Zhigilei, Phys. Rev. B **68**, 064114 (2003)
38. G. Galli, R.M. Martin, R. Car, M. Parrinello, Phys. Rev. Lett. **63**, 988 (1989)
39. P.L. Silvestrelli, A. Alavi, M. Parrinello, D. Frenkel, Phys. Rev. Lett. **77**, 3149 (1996)
40. A. De Vita, G. Galli, A. Canning, R. Car, Nature (Lond.) **379**, 523 (1996)
41. P.L. Silvestrelli, M. Parrinello, J. Appl. Phys. **83**, 2478 (1998)
42. C.Z. Wang, K.M. Ho, M.D. Shirk, P.A. Molian, Phys. Rev. Lett. **85**, 4092 (2000)
43. H.O. Jeschke, M.E. Garcia, K.H. Bennemann, Phys. Rev. B **60**, R3701 (1999)
44. H.O. Jeschke, M.E. Garcia, K.H. Bennemann, Appl. Phys. A **69**, 49 (1999)
45. H.O. Jeschke, M.E. Garcia, K.H. Bennemann, J. Appl. Phys. **91**, 18 (2002)
46. H.O. Jeschke, M.E. Garcia, M. Lenzner, J. Bonse, J. Krüger, W. Kautek, Appl. Surf. Sci. **197–198**, 839 (2002)
47. M.E. Garcia, H.O. Jeschke, Appl. Surf. Sci. **208–209**, 61 (2003)
48. H.O. Jeschke, M.E. Garcia, K.H. Bennemann, Phys. Rev. Lett. **87**, 015003 (2001)
49. H.O. Jeschke, M.E. Garcia, Appl. Surf. Sci. **197–198**, 107 (2002)
50. H.O. Jeschke, M.E. Garcia, J.A. Alonso, Chem. Phys. Lett. **352**, 154 (2002)
51. T. Dumitrica, M.E. Garcia, H.O. Jeschke, B.I. Yakobson, Phys. Rev. Lett. **92**, 117401 (2004)
52. A.H. Romero, M.E. Garcia, F. Valencia, M. Terrones, H. Terrones, H.O. Jeschke, Nano Lett. **5**, 1361 (2005)
53. J.S. Graves, R.E. Allen, Phys. Rev. B **58**, 13627 (1998)
54. T. Dumitrica, J.S. Graves, R.E. Allen, Phys. Rev. B **58**, 15340 (1998)
55. T.A. Halgren, J. Am. Chem. Soc. **114**, 7827 (1992)
56. J. Tersoff, Phys. Rev. B **37**, 6991 (1988)
57. F. Stillinger, T.A. Weber, Phys. Rev. B **31**, 5262 (1985)
58. C.H. Xu, C.Z. Wang, C.T. Chan, K.M. Ho, J. Phys. Condens. Mater. **4**, 6047 (1992)
59. M. van Schilfgaarde, W.A. Harrison, Phys. Rev. Lett. **67**, 3487 (1971)
60. M. Menon, J. Phys.: Condens. Matter **10**, 10991 (1998)
61. W.H. Knox, D.S. Chemla, G. Livescu, J.E. Cunningham, J.E. Henry, Phys. Rev. Lett. **61**, 1290 (1988)
62. T. Elsaesser, J. Shah, L. Rota, P. Lugli, Phys. Rev. Lett. **66**, 1757 (1991)
63. W. Woerner, W. Frey, M.T. Portella, C. Ludwig, T. Elsaesser, W. Kaiser, Phys. Rev. B **49**, 17007 (1994)
64. M. Parrinello, A. Rahman, Phys. Rev. Lett. **45**, 1196 (1980)
65. M. Parrinello, A. Rahman, J. Appl. Phys. **52**, 7182 (1981)
66. A.J. Stone, D.J. Wales, Chem. Phys. Lett. **128**, 501 (1986)
67. A. Hashimoto, K. Suenaga, A. Gloter, K. Urita, S. Iijima, Nature (Lond.) **430**, 870 (2004)
68. H.J. Choi, J. Ihm, S.G. Louie, M.L. Cohen, Phys. Rev. Lett. **84**, 2917 (2000)
69. M.S. Dresselhaus, G. Dresselhaus, P. Avouris (eds.), *Carbon Nanotubes: Synthesis, Structure, Properties and Applications*. Topics in Applied Physics, vol. 80 (Springer, Berlin, 2001)
70. E. Kaxiras, K.C. Pandey, Phys. Rev. Lett. **61**, 2693 (1988)
71. F. Valencia, A.H. Romero, H.O. Jeschke, M.E. Garcia, Phys. Rev. B **74**, 075409 (2006)
72. H.O. Jeschke, A.H. Romero, M.E. Garcia, A. Rubio, Phys. Rev. B **75**, 125412 (2007)
73. A. Togo, FROPHO, http://fropho.sourgeforge.net/
74. G. Nilsson, G. Nelin, Phys. Rev. B **3**, 364 (1970)